


**Quantum phase transition of a two-dimensional Rydberg atom array in an optical cavity**

Gao-Qi An and Yan-Hua Zhou

*Department of Physics and Chongqing Key Laboratory for Strongly Coupled Physics, Chongqing University, Chongqing 401331, China*Tao Wang <sup>\*</sup>*Department of Physics and Chongqing Key Laboratory for Strongly Coupled Physics, Chongqing University, Chongqing 401331, China  
and Center of Modern Physics, Institute for Smart City of Chongqing University in Liyang, Liyang 213300, China*

Xue-Feng Zhang

*Department of Physics and Chongqing Key Laboratory for Strongly Coupled Physics, Chongqing University, Chongqing 401331, China  
and Center of Quantum Materials and Devices, Chongqing University, Chongqing 401331, China*

(Received 20 April 2022; revised 29 August 2022; accepted 28 September 2022; published 11 October 2022)

We study the two-dimensional Rydberg atom array in an optical cavity with the help of a variational method and large-scale quantum Monte Carlo simulations. The strong dipole-dipole interactions between Rydberg atoms can make the system exhibit a crystal structure, and the coupling between a two-level atom and a cavity photon mode can result in the formation of a polariton. The interplay between them provides a rich quantum phase diagram including the Mott, solid-1/2, superradiant, and superradiant solid (SRS) phases. As a two-order coexisted phase, the superradiant solid breaks both translational and U(1) symmetries. Different from the fragile SRS phase in a one-dimensional system [Zhang *et al.*, *Phys. Rev. Lett.* **110**, 090402 (2013)], the SRS phase stays in a larger parameter region. Thus, it is more feasible to detect a SRS phase and corresponding quantum criticality in the real system involving dissipations. Our work not only extends the understanding of the light-atom interacting system, but also provides the guidelines and benchmark for the future experiments.

DOI: [10.1103/PhysRevB.106.134506](https://doi.org/10.1103/PhysRevB.106.134506)**I. INTRODUCTION**

Bringing a strong long-range interaction into a quantum simulator is a key topic, because it is important for studying the quantum phase transition (QPT) in a strongly correlated system [1]. As one of the most possible candidates, the Rydberg atoms stay at a high level state with large principal quantum number  $n$ , so that they possess two main advantages: a long lifetime ( $\approx 100 \mu\text{s}$  at  $n \approx 50$ ) and a strong long-range dipole-dipole interaction [2]. In order to simulate the quantum many-spin system, the Rydberg atoms are first loaded into the optical lattice [3,4]. However, in contrast to the small lattice length ( $< 1 \mu\text{m}$ ), the blockade radius of a Rydberg atom is so large (typically  $R_6 > 5 \mu\text{m}$ ) that few atoms can be excited to the Rydberg state [5,6]. Recently, due to the rapid development of optical tweezer arrays, a Rydberg atom can be trapped in each tweezer site with arbitrary geometry [7,8]. The programmable Rydberg atom array boosts the whole field, such as the gauge theory [9,10], quantum topological phase [11,12], the nonequilibrium quantum many-body system [13], and so on [14]. However, here the laser lights are taken as a classical light field, so the corresponding Hamiltonian is more like “classic.”

On the other hand, a quantized light field can be introduced by loading the ultracold atoms into an optical high-finesse

cavity [15]. Then, the interactions between atoms and photons are strongly amplified [16,17], and some exotic quantum phases emerge, such as a “supersolid” phase [18] and a superradiant phase [19]. Although some of them belong to quantum few-body systems, the theory and numerical simulation demonstrate that the generalized scaling relation of a QPT can still be detected [20–24].

Inspired by the recent experimental progress in both Rydberg atom arrays and cavity QED, it is valuable to discuss the QPT of a Rydberg atom array in an optical cavity. In our previous study [25], because of the interplay between a photon-mediated interaction and a dipole-dipole interaction, the superradiant solid (SRS) phase is found via large-scale numerical simulation. This quantum phase breaks both translational symmetry and U(1) symmetry, which is reminiscent of a “supersolid” phase. However, possibly due to the strong fluctuation in low dimension, the parameter region of the SRS phase is so narrow that it is hardly experimentally detected. Meanwhile, the fragility of the SRS phase also hinders the analysis of the associated quantum criticality in both theory and experiment.

In this paper, we study the QPT of a two-dimensional Rydberg atom array in a cavity shown in Fig. 1(a). By using both analytic approaches and large-scale quantum Monte Carlo (QMC) simulation, we determine the phase diagram comprised of the Mott insulator, solid-1/2, superradiant (SR), and SRS phases. The configuration of these phases is illustrated in Figs. 1(b)–1(e). In comparison with a one-dimensional case

<sup>\*</sup>Corresponding author. [tauwaang@cqu.edu.cn](mailto:tauwaang@cqu.edu.cn)

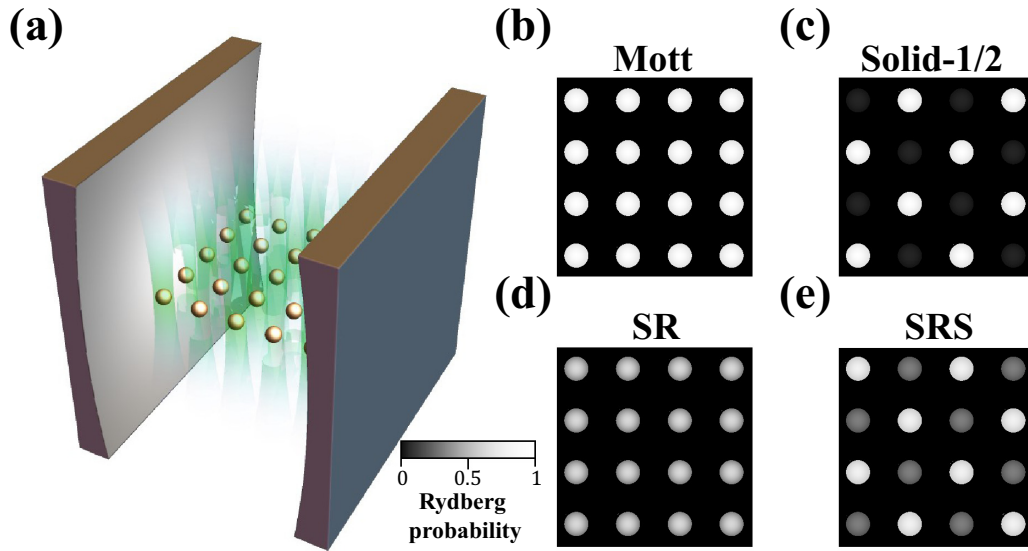


FIG. 1. (a) A schematic of a two-dimensional Rydberg atom array in a cavity. (b)–(e) Demonstrations of *in situ* Rydberg probability at different quantum phases in  $4 \times 4$  arrays.

[25], the region of the SRS phase becomes broad, which is extremely important for the experimental measurement. Meanwhile, the type of phase transition is analyzed in detail, especially the triple points.

The paper is organized as follows. In Sec. II, we discuss the model and its relation to both the Dicke model and the Ising model. In Sec. III, the variational method is borrowed to obtain the phase diagrams. In Sec. IV, we implement the QMC method and compare the numerical results with the analytic results. In Sec. V, we discuss the difference between one-dimensional (1D) and two-dimensional (2D) systems. Finally, in Sec. VI, we make the conclusion and discuss the relevance to the experiment.

## II. MODEL

In the experiment [2], the ultracold atom can be loaded into the defect-free tweezer arrays, and the Rydberg state can be excited via a two-photon transition. If the transition between the intermediate state  $|m\rangle$  and the ground state  $|g\rangle$  couples to a single quantized cavity mode, the whole system can be described by the following Hamiltonian [25,26]:

$$H = \frac{g}{\sqrt{N}} \sum_{i=1}^N (b_i^\dagger \psi + \text{H.c.}) + V \sum_{\langle i,j \rangle} n_i n_j - \Delta \sum_{i=1}^N n_i - \mu N_t, \quad (1)$$

where  $\psi^\dagger$  ( $\psi$ ) is the creation (annihilation) operator of photons;  $b_i^\dagger$  ( $b_i$ ) is the creation (annihilation) operator of the Rydberg atom at site  $i$ ;  $n_i = b_i^\dagger b_i$  is the local Rydberg density operator;  $\Delta \geq 0$  is the energy gap, which can be changed by adjusting the laser detuning;  $\mu$  is the chemical potential in the grand canonical ensemble;  $g$  is the effective atom-photon coupling strength, which is related to the cavity parameter and the Rabi frequency of transition between the Rydberg state

$|e\rangle$  and the intermediate state  $|m\rangle$ ;  $V$  denotes the strength of the dipole-dipole interactions between Rydberg atoms [27]; and  $\langle i, j \rangle$  represents that only a nearest-neighbor interaction is considered. The maximum occupation number at Rydberg state in each tweezer site should be 1, so  $b$  should be treated as a hard-core boson operator, and Eq. (1) is equivalent to the Hamiltonian in Ref. [25] (see Appendix A). It is obvious that the total density  $N_t \equiv \psi^\dagger \psi + \sum_{i=1}^N n_i$  is a conserved quantity. Meanwhile, the model preserves the U(1) symmetry, which is  $\psi^\dagger \rightarrow \psi^\dagger e^{i\theta}$  and  $b^\dagger \rightarrow b^\dagger e^{-i\theta}$ . Notice that the chemical potential  $\mu$  should be  $\leq 0$ , otherwise the number of photons will diverge.

In the weak interaction limit  $V \rightarrow 0$ , the model changes into the Dicke model within rotating wave approximation [28,29]. To avoid the divergence of total density, the chemical potential is set to be negative. Then, if the magnitude of the atom-photon coupling  $g$  is small, the system is in the normal phase or Mott-0 phase in which all the atoms stay in the ground state. On the other hand, when  $g$  is large, the atom and photon can form the polariton, so that the system enters into the SR phase which breaks the U(1) symmetry [Fig. 1(d)]. At critical point  $g_c = \sqrt{|\mu(\mu + \Delta)|}$ , a second-order QPT occurs.

In the strong interaction limit  $g \rightarrow 0$ , the photon mode is decoupled with the Rydberg atoms. Then, the Hamiltonian can be reduced to the Ising model by implementing the conventional mapping between hard-core boson and spin-1/2 operators  $b_i^\dagger \rightarrow S_i^+$ ,  $b_i \rightarrow S_i^-$ , and  $n_i \rightarrow S_i^z + 1/2$ . Then, the quantum phase diagram at zero temperature can be exactly obtained by calculating the energy of different configurations. When  $\mu < -\Delta$ , all atoms are at the ground state, i.e., the Mott-0 phase. After increasing  $\mu$  to be larger but less than  $4V - \Delta$ , the atoms on one sublattice are excited to the Rydberg state [Fig. 1(c)], so the translation symmetry is spontaneously broken and the solid-1/2 phase (antiferromagnetic phase in spin language) is constructed. Then, continuously increasing  $\mu$  to  $> 4V - \Delta$  results in the atoms being excited

to the Rydberg state, and the system enters into the Mott-1 phase [Fig. 1(b)].

In the intermediate region, the atom-photon coupling can provide a photon-mediated long-range interaction, so that the SRS phase emerges accompanied with both U(1) and translational symmetry spontaneously broken. In comparison with previous work [25], the Hamiltonian (1) is a hybrid 0D-2D quantum system, so the effect of the quantum fluctuation should be strongly different. The effect of dimension should strongly change the whole quantum phase diagram including the QPT. Thus first, we prefer to study the model with the help of the variational method.

### III. VARIATIONAL METHOD

The simplest variational wave function of ground state is taking the quantum spin as the classical one, and then finding the orientation of spins with the lowest energy. Such variational method is also suitable for our model, because the Rydberg atom is kind of quantum spin-1/2 as mentioned before. Meanwhile, since the coherent state is the ‘‘most classical’’ quantum state, we introduce following ansatz of wave function [25]:

$$|\lambda, \theta\rangle = e^{\lambda\sqrt{N}\psi^\dagger/2} \prod_i \left[ \cos\left(\frac{\theta_i}{2}\right) b_i^\dagger + \sin\left(\frac{\theta_i}{2}\right) \right] |0\rangle, \quad (2)$$

in which  $|0\rangle$  represents the vacuum state, and  $\lambda$  and  $\theta_i$  are the variational parameters of the photon and Rydberg atoms. Because only the nearest-neighbor repulsive interaction is kept, the translational symmetry breaking can only result in the Néel order or the  $(\pi, \pi)$  order. Thus, we set the variables  $\theta_i$  to be the same in the same sublattice  $C$  or  $D$ , then the only variational parameters remaining are only left with  $(\lambda, \theta_C, \theta_D)$ . The energy per site of the ansatz Eq. (2) can be calculated as  $E = \langle \lambda, \theta | H | \lambda, \theta \rangle / N$  and

$$4E = g\lambda(\sin\theta_C + \sin\theta_D) + 2V \cos\theta_C \cos\theta_D - \mu\lambda^2 - (\mu + \Delta - 2V)(\cos\theta_C + \cos\theta_D) + E_0, \quad (3)$$

where  $E_0 = -2(\mu + \Delta - V)$  is energy constant.

The ground state can be calculated by minimizing the energy per site  $E$  with respect to the variational parameters  $\lambda$ ,  $\theta_C$ , and  $\theta_D$ . The system has the sublattice symmetry  $C \leftrightarrow D$ . Considering that the ground states of the solid-1/2 and SRS phases have twofold degeneracy, we can set  $0 \leq \theta_D \leq \theta_C < 2\pi$  without loss of generality. The population of atoms at the Rydberg state or Rydberg probability can be evaluated by  $\rho_i = [\cos(\theta_i) + 1]/2$ . When the density  $\rho_C$  is not equal to  $\rho_D$ , it means that the translational symmetry is spontaneously broken. In addition, the energy is unchanged under the transformation  $\lambda \rightarrow -\lambda$  and  $(\theta_C, \theta_D) \rightarrow -(\theta_C, \theta_D)$ , so the photon parameter is set to  $\lambda \geq 0$ . Because the ansatz is the coherent state, the expectation of photon density is  $|\lambda|^2$ . Then, the nonzero  $\lambda$  indicates the U(1) symmetry is spontaneously broken. Without loss of generality, we take  $V$  as the unit of energy and set it to 1.

In Fig. 2, we show the Rydberg probabilities in different sublattices and photon parameter  $\lambda$  at different  $\Delta$ . When  $\mu$  is much smaller, all the atoms stay at the ground state without photons in the cavity, and it is the Mott-0 phase.

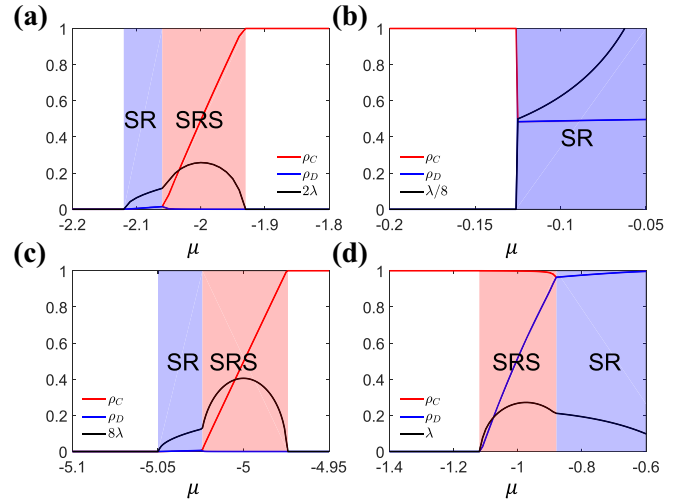


FIG. 2. Rydberg probabilities in different sublattices and the variational parameter of photon  $\lambda$  are calculated at different chemical potentials  $\mu$  with the help of the variational method. The atom-photon coupling strength is chosen  $g = 0.5$  with (a),(b)  $\Delta = 2$  and (c),(d)  $\Delta = 5$ . The regions of the SR and SRS phases are highlighted with different colors.

After increasing the chemical potential  $\mu$  to a certain critical value, the photon number starts increasing and the Rydberg probabilities in both sublattices turn out to be finite and equal. These phenomena demonstrate that the quasiparticle polaritons are excited and break the U(1) symmetry, so that the SR phase emerges. Then, similar to the one-dimensional case [25], the larger  $\mu$  cannot immediately drive the system into the solid-1/2 phase. Instead of this, the exotic SRS phase can be found between the SR and solid-1/2 phases. From the order parameters in the SRS phase shown in Figs. 2(a) and 2(c), we can find both the photon numbers and the Rydberg probabilities are finite, but different from the SR phase, the Rydberg probabilities in both sublattices are different. This means that, as the two-order coexisted phase, the SRS phase breaks both U(1) and translational symmetries. In the strong-coupling limit  $g \ll \Delta$ , the SRS phase can be understood as follows: the atoms in one sublattice couple the photons and construct the polaritons [30]. While approaching the solid-1/2 phase, the photon density is dropping down to zero. In the solid-1/2 phase, only the atoms in one sublattice are excited to the Rydberg state, and no photons exist in the cavity at the same time.

However, when continuously increasing the chemical potential  $\mu$ , the existence of the SRS phase is related to the magnitude of the energy gap  $\Delta$ . When the gap is small, such as  $\Delta = 2$  in Fig. 2(b), the SRS phase is unstable, so that the QPT between the SR and the solid-1/2 phase is first order. It can be obviously reflected by the jump of the Rydberg probabilities and the photon density. In comparison, the large energy gap [see Fig. 2(d)] can stabilize the SRS phase, in which the atoms of one sublattice are almost fully polarized and the other sublattice is occupied with the polaritons. Furthermore, the QPTs among the SR, SRS, and solid-1/2 phases are all second order, which is the same as the situation at lower chemical potentials.

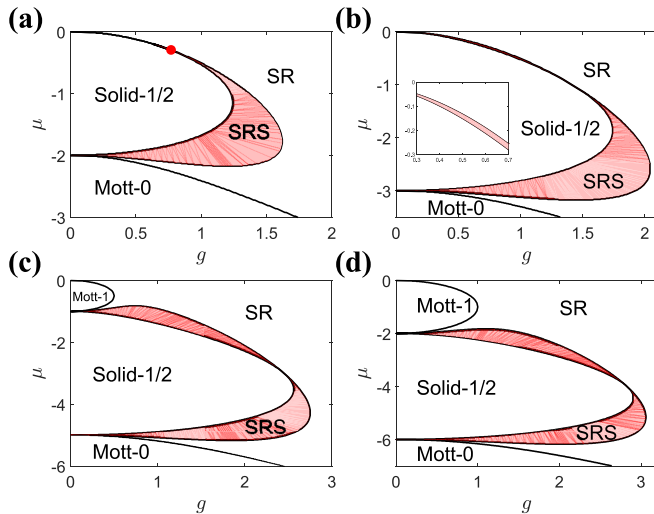


FIG. 3. Quantum phase diagram calculated from the variational method at different gap energy (a)  $\Delta = 2$ , (b)  $\Delta = 3$ , (c)  $\Delta = 5$ , and (d)  $\Delta = 6$ . The region of the SRS phase is marked with in red, and the red dot points out the triple point. Inset: the phase diagram at  $\Delta = 3$  after zooming in.

The whole quantum phase diagram in the  $\mu$ - $g$  panel with different gap energy  $\Delta$  is drawn in Fig. 3. In both strong- and weak-coupling regions, the solid-1/2, Mott, and SR phases follow the analysis mentioned before. In the intermediate region, the quantum phase diagram becomes rich. Apparently, the gap energy can stabilize the solid-1/2 and Mott phase, so that their regions are enlarged while increasing  $\Delta$ . When the gap energy is small [Fig. 3(a) at  $\Delta = 2$ ], the solid-1/2 phase has two selections for entering the SR phase: (i) a direct first-order phase transition through the upper phase boundary; and (ii) two successive second-order phase transitions through the lower intermediate SRS phase. Meanwhile, there is a triple point among these phases [red dot in Fig. 3(a)]. Then, while increasing  $\Delta$ , the upper SRS phase emerges and its region is expanding. However, the upper and lower regions of the SRS phase are not connected, and it hints that there are two triple points jointed with first-order phase transition or one quadruple point. To address these questions and to quantitatively study this system, we require a more accurate method, like the quantum Monte Carlo simulation method.

#### IV. QUANTUM MONTE CARLO SIMULATION

The numerical method we adopted is the stochastic series expansion method [31,32]. Different from the conventional algorithm, here the operator vertex includes three Rydberg sites and one photonic mode site. Meanwhile, the maximum occupation number of photons is adjusted to always be much higher than the possible photon number during the simulation, so there is no system error caused by the truncation, and the algorithm in details can be found in the Supplemental Material of Ref. [25]. The inverse temperature is set to  $\beta = 1/T = 100$ , so that it is much lower than the other energy scales ( $k_B = 1$ ). The system size simulated is up to  $20 \times 20 = 400$  sites, which is much larger than the real system ( $\approx 250$  [8]).

Usually, the distance between nearest-neighbor sites in the experiment is around  $5 \mu\text{m}$ , so the system size  $20 \times 20$  implies the size of the cavity has to be larger than  $100 \mu\text{m}$  at least. However, it is not an easy task even with state-of-the-art techniques. In addition, we choose the periodic boundary condition. The possible quantum phases can be divided into two categories: (1) the solid-1/2 and Mott phases are incompressible; (2) the SRS and SR phases are compressible. Thus, we introduce the compressibility  $\kappa = N\beta(\langle \rho^2 \rangle - \langle \rho \rangle^2)$  to distinguish them, in which  $\rho = \sum_{i=1}^N n_i/N$  is the average Rydberg probability. For the incompressible phases, the Mott phases keep the integer filling and the solid-1/2 phase corresponds to half-filling. Now let us consider the compressible phase; the SRS phase further breaks the translational symmetry while the SR phase does not. Thus, the structure factor  $S(\mathbf{Q})/N = \langle |\sum_{i=1}^N n_i e^{i\mathbf{Q}\cdot\mathbf{R}_i}|^2 \rangle / N^2$  is taken as the order parameter to characterize the translational symmetry breaking. In the solid-1/2 phase, the same as the Néel phase in the magnetic materials, the corresponding  $\mathbf{Q}$  is equal to  $(\pi, \pi)$ . Then, the value of  $S(\mathbf{Q})/N$  of solid-1/2 is exactly 1/4 at  $g = 0$ , because the Rydberg probability is equal to 1 in one sublattice and zero in the other. Meanwhile, it should be a finite value in the SRS phase and zero in the other phases.

The QPT between the solid-1/2 and the SRS phase can be clearly identified in Fig. 4 at large chemical potential  $\mu = -2.5$  with small gap energy  $\Delta = 3$ . When the coupling  $g$  is small, the compressibility  $\kappa$  is zero and the structure factor  $S(\mathbf{Q})/N$  is almost 0.25, so the system is in the solid-1/2 phase. Meanwhile, the zero photon density  $\rho_a = \psi^\dagger \psi$  in Fig. 4(b) demonstrates that no photon exists in the optical cavity. Then, the same as the prediction of the variational method, numerous polaritons are excited and prefer one sublattice, so we can observe that both  $S(\mathbf{Q})/N$  and  $\kappa$  are finite in the SRS phase which breaks two symmetries. The photon density with different system sizes can be scaled to one line by dividing the number of Rydberg sites  $N$  [see Fig. 4(b)], and it hints that the polariton density is nearly unchanged while enlarging the system size. In other words, the average photon numbers for constructing the polariton is almost the same at different sizes. Furthermore, all the smooth curves of different observables demonstrate that the QPT is second order.

Although the variational method supports that the QPT between the SRS and SR phases is continuous, the numerical results in other similar systems are different [25,30]. In Fig. 4, we can find the QPT looks continuous at a small system size, such as  $L = 10$ , but the structure factor suddenly jumps to  $\approx 0$  at the critical point  $g_c = 1.76$  for larger sizes. At the same time, such small discontinuity can also be observed from the photon density  $\rho_a$ . Most importantly, as shown in Fig. 4(a), the values of  $\kappa$  at the peak increase along with the system size and tend to diverge. In contrast, it is decreasing at  $g$  slightly larger than  $g_c$  (black arrow highlights). To further verify the type of QPT, we calculate the Binder cumulant defined as  $S_b = 1 - \frac{\langle S(\mathbf{Q})^2 \rangle}{3\langle S(\mathbf{Q}) \rangle^2}$  and plot it in Fig. 4(b). It is zero in the SR phase, and about 2/3 in the ordered phase (both the solid-1/2 and SRS phases break the translational symmetry). When  $g$  is close to the critical point  $g_c$ , the Binder cumulant also presents a clear jump at a larger size, and it indicates the QPT is first order.

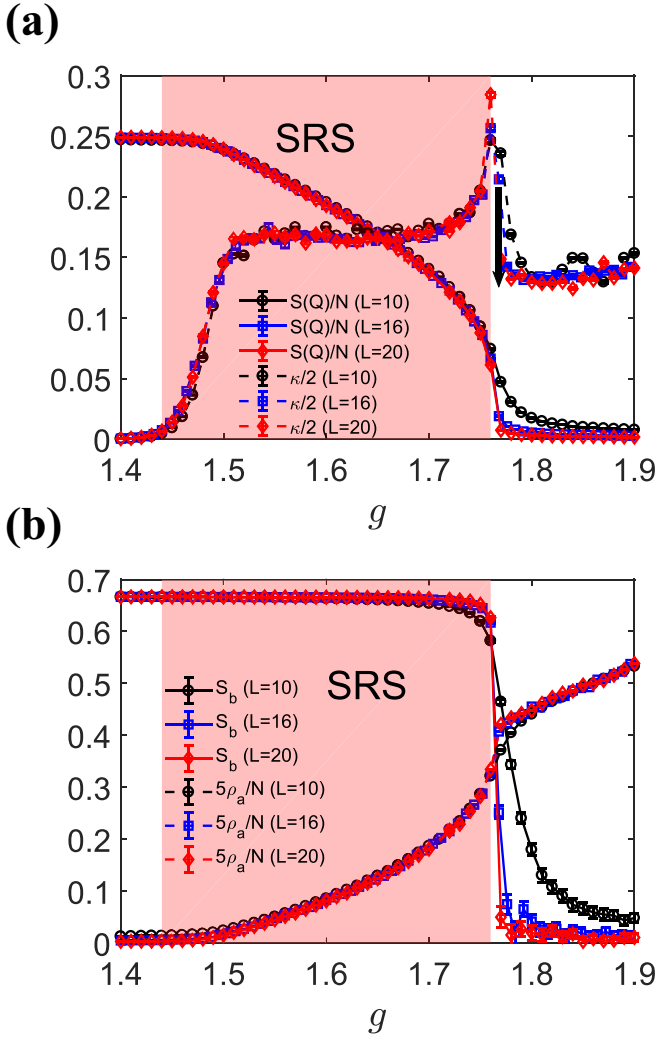


FIG. 4. (a) The structure factor  $S(\mathbf{Q})/N$  and the compressibility  $\kappa$ . (b) The Binder cumulant  $S_b$  and the photon density  $\rho_a$  at  $\Delta = 3$  and  $\mu = -2.5$  with different system sizes obtained by QMC simulation. The region of the SRS phase is marked with red. The black arrow highlights the decrease of  $\kappa$  near the critical point.

When the chemical potential  $\mu$  becomes smaller, as shown in Fig. 5(a), the region of the SRS phase shrinks. Meanwhile, the first-order phase transition between the SRS and the SR phase turns out to be more apparent, and we can observe obvious jumps of all the observables. However, different from the prediction of the variational method at  $\Delta = 3$ , the QPT between the solid-1/2 and the SR phase turns out to be direct first order in Fig. 5(b). Indeed, such phenomenon also exists for the results of the variational method at small  $\Delta$ , and it reflects that the variational method underestimates the quantum fluctuations as usual. In the real system, the largest number of tweezer sites is around  $\approx 200$ . Thus, instead of tediously achieving the phase diagram in the thermodynamic limit, it is more practical to obtain the “finite-size phase diagram.” Here, the system size of the phase diagram is  $N = 100$ . The phase boundary of the incompressible phase is set to the value at which the compressibility  $\kappa$  is just larger than  $10^{-3}$ . Meanwhile, the finite-size phase boundary between the SRS and the

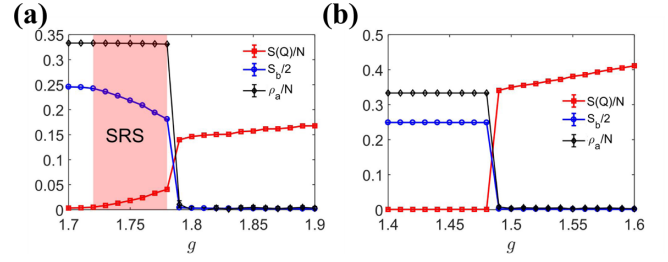


FIG. 5. The structure factor  $S(\mathbf{Q})/N$ , its Binder cumulant  $S_b$ , and the photon density  $\rho_a$  at  $\Delta = 3$  with system size equal to  $L = 20$  obtained by QMC simulation. The chemical potential is set to (a)  $\mu = -2.1$  and (b)  $\mu = -1.2$ . The region of the SRS phase is marked with red.

SR phase is found by the singularity of  $\kappa$ . From the quantum phase diagram at  $\Delta = 3$  in Fig. 6, we can find the region of the SRS phase is slightly smaller than the variational method phase diagram. This indicates that the system behaves more “classically.” In comparison with the one-dimensional case, the SRS phase is more stable, so that it will be more accessible in the real experiment. Meanwhile, it should be also possible to detect the triple point among the SRS, SR, and solid-1/2 phases.

On the other hand, the critical lines of the second-order QPT of the incompressible phases can also be calculated via the perturbation theory, which is also known as the strong-coupling expansion (SCE) method [33,34]. Several works have demonstrated that it can provide very accurate results comparable to the numerical results. The phase boundary of the Mott-0 phase can be calculated by comparing the vacuum energy with the perturbative energy of one polariton excited state, and the second-order result is  $\mu = -\Delta - g^2/\Delta$ . The QPT from the solid-1/2 to the SRS phase is second order, but the upper and lower critical lines should be discussed separately. The lower one is caused by the “holelike” excitations. When the chemical potential is smaller than the critical line, one atom at the Rydberg state can go back to the ground state and form a “hole.” Then, as the quasiparticle, the polariton can

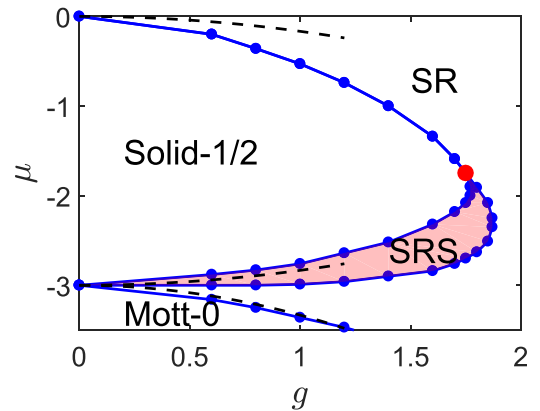


FIG. 6. The phase diagram at  $\Delta = 3$  and  $L = 10$ . The blue dotted lines are the phase boundaries obtained with QMC simulations, and the dashed lines are the analytic results of the strong-coupling expansion method. The region of the SRS phase is shaded with red, and the red dot marks the triple point.

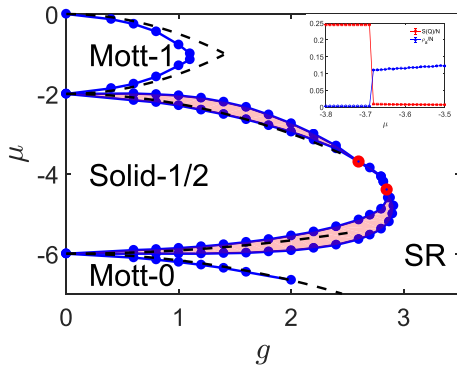


FIG. 7. The phase diagram at  $\Delta = 6$  and  $L = 10$ . The blue dotted lines are the phase boundaries obtained with QMC simulations, and the dashed lines are the analytic results of the strong-coupling expansion method. The region of the SRS phase is shaded with red, and the red dots mark the triple points. Inset: the structure factor and photon density for different  $\mu$  at  $g = 2.6$ .

also be composed of the hole and photon. Thus, the energy difference between a single “hole-polariton” excited state and a solid-1/2 phase can give the second-order lower critical line  $\mu = -\Delta + g^2/2\Delta$ . For the upper boundary at  $\Delta < 4$ , the first excited state is with an additional photon, so the critical line is  $\mu = -g^2/2\Delta$ .

We compare the SCE results with the numerical result in Fig. 6, and the critical lines of the Mott-0 phase quantitatively match well, and so do the lower boundaries of QPT between the SRS and solid-1/2 phases. However, the upper boundary shows a large discrepancy, because the melting of the solid-1/2 phase becomes first order. Inspired by both numerical and analytical results, we find it is hard to produce the upper SRS phase when  $\Delta < 4V$ . One possible mechanism may be understood as follows: it is hard to excite the atom to the Rydberg state in the solid-1/2 phase when  $\Delta < 4V$ , so it is also difficult to construct the polaritons even with photons in the optical cavity.

At last, we simulate the QPT at large gap energy  $\Delta = 6$ , and the quantum phase diagram is shown in Fig. 7. The Mott-1 phase appears at high chemical potential. In the Mott-1 phase, all the atoms stay at the Rydberg state, and the upper and lower boundaries can be obtained by calculating the perturbative energies of the single “particle-polariton” or the “hole-polariton” excited state. Then, the SCE method gives the second-order upper critical line  $\mu = -g^2/(\Delta - 4V)$  and the lower one  $\mu = -(\Delta - 4V) + g^2/(\Delta - 4V)$ . In Fig. 7, we can find that the critical lines of the Mott-1 phase from both QMC and SCE methods match well at small  $g$ , and seem to be symmetric along  $\mu = -1$ , which may correspond to the hidden particle-hole symmetry. Furthermore, because the gap energy  $\Delta$  is larger than  $4V$ , the SRS phase reappears with particle-polariton excitation. Then, the second-order upper critical line of the QPT between the solid-1/2 and the SRS phase changes to  $\mu = -(\Delta - 4V) - g^2/2(\Delta - 4V)$ . In Fig. 7, all the critical lines from the SCE method are very close to the numerical results at small  $g$ , and it demonstrates that the physical mechanism of polariton excitation driving the QPT is appropriate. Finally, between the SRS phases, there are two triple points linked with first-order phase transition (see the

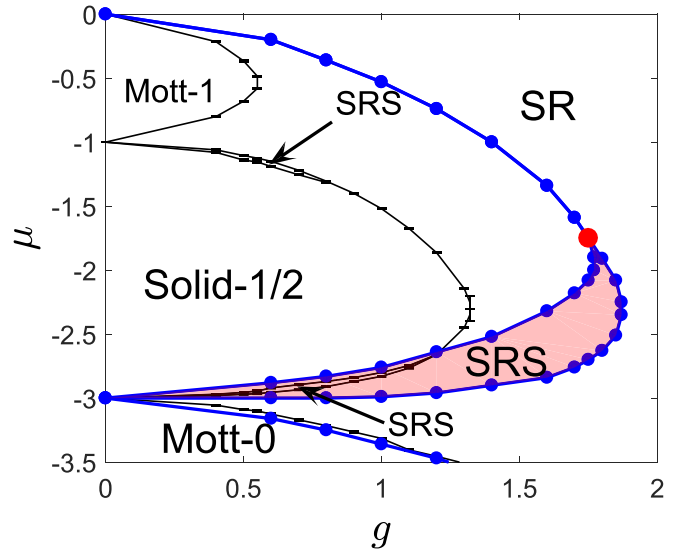


FIG. 8. The quantum phase diagrams of Rydberg atom array in square lattice (blue dot line) and 1-d chain (black line) with same detuning  $\Delta = 3$  and number of sites  $N = 100$ . The region of SRS phase in 1-d chain is pointed out by the black arrows. All the data are obtained by QMC simulations

inset of Fig. 7), which is also found in the one-dimensional system [25].

## V. COMPARISON OF 1D AND 2D SYSTEMS

In the strongly correlated system, the dimension plays a critical role in the quantum phase transition [35]. Therefore, it is worth comparing the two-dimensional system with the one-dimensional chain [25]. Here, we choose the same detuning  $\Delta = 3$  and number of sites  $N = 100$ . In Fig. 8, the discrepancy of the quantum phase diagram between different dimensions can be clearly exhibited.

The major difference between the 1D and 2D systems is the region of the SRS phase. In previous work [25], the numerical simulation demonstrates that the SRS phase in 1D will always exist in an extremely tiny region, no matter how the system parameter changes. Nevertheless, in a real system, such fragile SRS phase may be destroyed by the photon leaking, the noise of lasers, the spontaneous emission of the Rydberg state, and the loss caused by the intermediate state during the two-photon transitions. In contrast, the SRS phase in 2D is stable in a large parameter region, so it can be easily detected in the real system and so is the triple point.

On the other hand, the upper SRS phase disappears in 2D at the same system parameters, but it can also be stable in a large parameter region at large detuning as shown in Fig. 7. This means that the SRS phases with different types of excitations can be observed in the realistic system, but also the corresponding triple point and even the more complicated quantum criticality.

Furthermore, it is technically hard to manufacture a larger cavity with high finesse, so the cavity can couple to more array sites in a two-dimensional system. Accordingly, since more array sites have less finite-size effect, it is more feasible to

identify the SRS phase and quantum phase transition in the 2D system.

## VI. CONCLUSION AND OUTLOOK

In conclusion, using the variational method, strong-coupling expansion method, and larger scale quantum Monte Carlo simulation, we obtain the quantum phase diagram of Rydberg atoms trapped in square tweezer arrays inside an optical cavity. Not only the Mott phase, solid-1/2, and SR phases are observed, most importantly, the SRS phase which breaks both symmetries is well analyzed. The transition between the SR and solid-1/2 phases can be the direct first-order, or the two successive second-order QPTs through the intermediate SRS phase. The existence of the upper SRS phase is clearly related to the gap energy, and so are the triple points among the SRS, SR, and solid-1/2 phases. The phase transition between the SRS and the SR phase is found to be first order, but we still cannot rule out the continuous one in the real system due to the size or edge effect.

Furthermore, the preparation of the quantum state is not a simple task. In Appendix B, we discuss it with the help of numerical simulation in a small system size. Considering the rapid progress that has been made in the fields of cavity and tweezers [7,8,16,17], our work will pave a way for experiments in the near future and certainly provide a benchmark for it at the same time.

## ACKNOWLEDGMENTS

X.-F. Z. is thankful for valuable discussions with Qin Sun. This work is supported by the National Science Foundation of China under Grant No. 12274045 and the China Postdoctoral Science Foundation Funded Project No. 2020M673118. X.-F.Z. acknowledges funding from the National Science Foundation of China under Grants No. 12274046, No. 11874094, and No.12147102, and Fundamental Research Funds for the Central Universities Grant No. 2021CDJZYJH-003.

## APPENDIX A: HAMILTONIAN WITH A SINGLE-OCCUPANCY CONSTRAINT

In the previous paper [25], the original model describing the system can be presented as

$$H = \omega_c \psi^\dagger \psi + \sum_{i=1}^N \frac{\epsilon}{2} (e_i^\dagger e_i - g_i^\dagger g_i) + \frac{g}{\sqrt{N}} \sum_{i=1}^N (e_i^\dagger g_i \psi + \text{H.c.}) + V \sum_{(i,j)} P_{ee}^{(i)} P_{ee}^{(j)} - \mu_t N_t, \quad (\text{A1})$$

where  $\omega_c$  and  $\epsilon$  are the cavity and atom transition frequencies with the detuning defined by  $\Delta = \omega_c - \epsilon$ .  $\psi$  is the single-mode creation operator of the cavity field;  $g_i$  and  $e_i$  are the boson operators representing the ground state and Rydberg state of each atom and satisfy the single-occupancy constraint  $e_i^\dagger e_i + g_i^\dagger g_i = 1$  and  $g$  is the effective two-photon coupling.  $P_{ee}^{(i)} = e_i^\dagger e_i$  are the projectors onto the Rydberg state with  $V$  being the strong dipole-dipole interactions between two nearest-neighbor sites. The last term is the chemical potential,

where  $N_t = \psi^\dagger \psi + \sum_{i=1}^N e_i^\dagger e_i$  denotes the total excitations of the systems. Some notations are changed to avoid ambiguity, such as  $b^\dagger \rightarrow e^\dagger$  and  $a^\dagger \rightarrow g^\dagger$ .

In the defect-free Rydberg atom array, each tweezer site is occupied by one atom which is called the single-occupancy constraint. With such constraint, the Rydberg atom can be described by the Pauli operators  $\sigma_i^+ = e_i^\dagger g_i$ ,  $\sigma_i^- = e_i g_i^\dagger$ ,  $\sigma_i^z = e_i^\dagger e_i - g_i^\dagger g_i$ , and  $P_{ee}^{(i)} = (1 + \sigma_i^z)/2$ . Then, the Hamiltonian, Eq. (A1), can be rewritten as

$$H = \omega_c \psi^\dagger \psi + \sum_{i=1}^N \frac{\epsilon}{2} \sigma_i^z + \frac{g}{\sqrt{N}} \sum_{i=1}^N (\sigma_i^+ \psi + \text{H.c.}) + V \sum_{(i,j)} (1 + \sigma_i^z)(1 + \sigma_j^z)/4 - \mu_t N_t. \quad (\text{A2})$$

Hereafter, we can implement the conventional mapping between hard-core boson operators and Pauli operators  $\sigma_i^+ \rightarrow b_i^\dagger$ ,  $\sigma_i^- \rightarrow b_i$ , and  $\sigma_i^z \rightarrow 2b_i^\dagger b_i - 1 = 2n_i - 1$ . Finally, Eq. (A2) changes into the Hamiltonian, Eq. (1), with  $\Delta = \omega_c - \epsilon$  and  $\mu = \mu_t - \omega_c$ .

## APPENDIX B: PREPARATION OF THE QUANTUM STATES

In the quantum simulation platform, the system is usually prepared in some trivial state, such as the ferromagnetic phase. In the Rydberg atom array, it is easy to prepare all the atoms in the ground state, which is the Mott-0 phase. However, preparation of other symmetry breaking phases, especially the SRS phase, is not a straightforward task. In particular, the timescale should be so short that the dissipative factors such as the photon leaking and spontaneous emission of Rydberg states can be neglected. In this section, we use the Runge-Kutta method to study the time evolution of our system and try to find acceptable procedures of state preparation.

### 1. Adiabatic evolution from Mott-0 to solid-1/2

The solid-1/2 phase or the Néel phase can be prepared with the help of adiabatic evolution of the Mott-0 phase, and it has been achieved in two-dimensional Rydberg optical tweezer arrays with more than 250 sites [8]. Differently, the laser fields of the two-photon transition are classical, so that the Hamiltonian is changed into

$$H(t) = \frac{\Omega(t)}{2} \sum_i (b_i^\dagger + b_i) - \Delta(t) \sum_i n_i + V \sum_{(i,j)} n_i n_j, \quad (\text{B1})$$

where  $\Omega$  and  $\Delta$  are the two-photon Rabi frequency and detuning, respectively. In order to get a high fidelity of target state by evolving the solid-1/2 state, as shown in the inset of Fig. 9, we adopt the similar setting [8] of  $\Omega(t)$  and  $\Delta(t)$  as

$$\Omega(t) = \begin{cases} 6Vt/t_0 & t/t_0 < 1/3 \\ 2V & 1/3 \leq t/t_0 < 2/3 \\ 6V(1-t/t_0) & 2/3 \leq t/t_0 < 1, \end{cases}$$

$$\Delta(t) = \begin{cases} -2V & t/t_0 < 1/3 \\ -6V(1-2t/t_0) & 1/3 \leq t/t_0 < 2/3 \\ 2V & 2/3 \leq t/t_0 < 1. \end{cases}$$

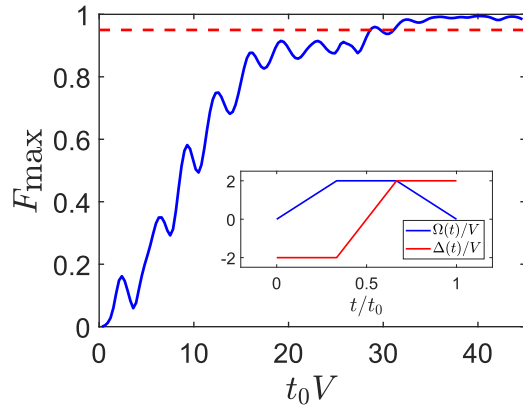


FIG. 9. The maximum of fidelity  $F_{\max}(t_0)$  as a function of  $t_0$ , while the Mott-0 state evolves into the target solid-1/2 state. The red dashed line marks the fidelity equal to 95%. Inset: the modulation function of detuning and Rabi frequency.

The system size of the Runge-Kutta time-dependent simulation is limited to  $4 \times 4$ , because the Hilbert space will exponentially explode while increasing the system size. The wave function of the target state  $|\phi_t\rangle$  can be obtained by solving the instant Hamiltonian  $H(t_0)$ , so that we can calculate the fidelity  $F(t) = \langle \phi(t) | \phi_t \rangle$  at different time  $t \in [0, t_0]$ . By varying the evolution time  $t_0$ , we can get the maximum of fidelity  $F_{\max}(t_0)$ . As shown in Fig. 9, the fidelity  $F_{\max}$  is larger than 95% while  $t_0$  is longer than  $\approx 30V^{-1}$ .

## 2. Adiabatic evolution from solid-1/2 to SRS

Considering the quantum phase transition from the solid-1/2 and SRS states is continuous, it should be faster to prepare the SRS state by evolving the solid-1/2 state. The simulation is in the canonical ensemble, so the time-dependent Hamiltonian is without the chemical potential part:

$$H = \frac{g(t)}{\sqrt{N}} \sum_{i=1}^N (b_i^\dagger \psi + \text{H.c.}) + V \sum_{\langle i,j \rangle} n_i n_j - \Delta \sum_{i=1}^N n_i. \quad (\text{B2})$$

Here, we set  $\Delta = 3V$  and  $g(t) = 1.8Vt/t_0$  ( $0 \leq t/t_0 \leq 1$ ), because the parameters correspond to the SRS phase according to the quantum phase diagram in Fig. 6. Meanwhile, the truncation of the photon numbers is set to be  $N_t$ , so no truncation error is introduced. In Fig. 10, we find the fidelity between the SRS and solid-1/2 phases is over 50% at starting time ( $t_0 = 0$ ). Meanwhile, similar to the evolution from Mott-0 to

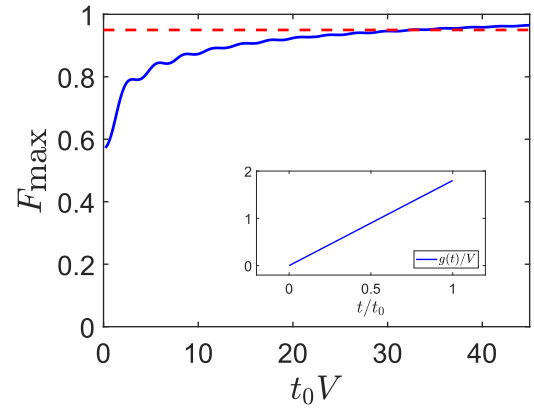


FIG. 10. The maximum of fidelity  $F_{\max}(t_0)$  as a function of  $t_0$ , while the solid-1/2 state evolves into the target SRS state. The red dashed line marks the fidelity equal to 95%. Inset: the modulation function of atom-photon coupling  $g$ .

solid-1/2, the maximum of fidelity  $F_{\max}$  is over 95% when the duration time  $t_0$  is longer than  $30V^{-1}$ .

## 3. Timescale of state preparation

In a real experiment, photon leaking will play an important role during the above processes of state preparation. In order to avoid the photon leaking, we could improve the quality of our cavity or shorten the time duration of state preparation. Taking the parameters of experiment [8] as the references, the principal number of the Rydberg state is set to be 70, the lattice spacing is  $a = 6.7$  nm, and the interaction  $V$  is around 10 MHz. Therefore, the timescale of preparing a state with more than 95% fidelity is around several microseconds. Considering the leaking rate of the cavity with ultrahigh finesse is less than megahertz [18,19], the corresponding influence should not be serious during the adiabatic preparation. However, it is still extremely hard for a larger system, because the quality of the cavity drops down fast while increasing its length.

As for the spontaneous emission of the Rydberg state, the lifetime is generally around  $100 \mu\text{s}$ . Therefore, a several microseconds state preparation is short enough to avoid the effect of spontaneous emission.

The atom losses from the intermediate state could be avoided by using the so-called adiabatic emission technique in the two-photon transition process. This method requires that the laser which couples the ground state and the intermediate state is far-detuned with the energy gap between the ground state and the intermediate state. As for the result, only a very small fraction of atoms are excited to intermediate energy levels and the losses from the intermediate state could be suppressed.

[1] F. Schäfer, T. Fukuhara, S. Sugawa, Y. Takasu, and Y. Takahashi, *Nat. Rev. Phys.* **2**, 411 (2020).

[2] A. Browaeys and T. Lahaye, *Nat. Phys.* **16**, 132 (2020).

[3] P. Schauß, M. Cheneau, M. Endres, T. Fukuhara, S. Hild, A. Omran, T. Pohl, C. Gross, S. Kuhr, and I. Bloch, *Nature (London)* **491**, 87 (2012).



- [4] P. Schauß, J. Zeiher, T. Fukuhara, S. Hild, M. Cheneau, T. Macrì, T. Pohl, I. Bloch, and C. Gross, *Science* **347**, 1455 (2015).
- [5] D. Comparat and P. Pillet, *J. Opt. Soc. Am. B* **27**, A208 (2010).
- [6] M. Saffman, T. G. Walker, and K. Mølmer, *Rev. Mod. Phys.* **82**, 2313 (2010).
- [7] P. Scholl, M. Schuler, H. J. Williams, A. A. Eberharter, D. Barredo, K.-N. Schymik, V. Lienhard, L.-P. Henry, T. C. Lang, T. Lahaye, A. M. Läuchli, and A. Browaeys, *Nature (London)* **595**, 233 (2021).
- [8] S. Ebadi, T. T. Wang, H. Levine, A. Keesling, G. Semeghini, A. Omran, D. Bluvstein, R. Samajdar, H. Pichler, W. W. Ho, S. Choi, S. Sachdev, M. Greiner, V. Vuletić, and M. D. Lukin, *Nature (London)* **595**, 227 (2021).
- [9] F. M. Surace, P. P. Mazza, G. Giudici, A. Leroise, A. Gambassi, and M. Dalmonte, *Phys. Rev. X* **10**, 021041 (2020).
- [10] R. Verresen, M. D. Lukin, and A. Vishwanath, *Phys. Rev. X* **11**, 031005 (2021).
- [11] S. de Léséleuc, V. Lienhard, P. Scholl, D. Barredo, S. Weber, N. Lang, H. P. Büchler, T. Lahaye, and A. Browaeys, *Science* **365**, 775 (2019).
- [12] G. Semeghini, H. Levine, A. Keesling, S. Ebadi, T. T. Wang, D. Bluvstein, R. Verresen, H. Pichler, M. Kalinowski, R. Samajdar, A. Omran, S. Sachdev, A. Vishwanath, M. Greiner, V. Vuletić, and M. D. Lukin, *Science* **374**, 1242 (2021).
- [13] C. J. Turner, J.-Y. Desaulles, K. Bull, and Z. Papić, *Phys. Rev. X* **11**, 021021 (2021).
- [14] A. M. Kaufman and K.-K. Ni, *Nat. Phys.* **17**, 1324 (2021).
- [15] H. Ritsch, P. Domokos, F. Brennecke, and T. Esslinger, *Rev. Mod. Phys.* **85**, 553 (2013).
- [16] K. Baumann, C. Guerlin, F. Brennecke, and T. Esslinger, *Nature (London)* **464**, 1301 (2010).
- [17] R. Mottl, F. Brennecke, K. Baumann, R. Landig, T. Donner, and T. Esslinger, *Science* **336**, 1570 (2012).
- [18] R. Landig, L. Hruby, N. Dogra, M. Landini, R. Mottl, T. Donner, and T. Esslinger, *Nature (London)* **532**, 476 (2016).
- [19] X. Zhang, Y. Chen, Z. Wu, J. Wang, J. Fan, S. Deng, and H. Wu, *Science* **373**, 1359 (2021).
- [20] M.-J. Hwang, R. Puebla, and M. B. Plenio, *Phys. Rev. Lett.* **115**, 180404 (2015).
- [21] M. Liu, S. Chesi, Z.-J. Ying, X. Chen, H.-G. Luo, and H.-Q. Lin, *Phys. Rev. Lett.* **119**, 220601 (2017).
- [22] H.-J. Zhu, K. Xu, G.-F. Zhang, and W.-M. Liu, *Phys. Rev. Lett.* **125**, 050402 (2020).
- [23] Y. Xu and H. Pu, *Phys. Rev. Lett.* **122**, 193201 (2019).
- [24] Y.-Y. Zhang, Z.-X. Hu, L. Fu, H.-G. Luo, H. Pu, and X.-F. Zhang, *Phys. Rev. Lett.* **127**, 063602 (2021).
- [25] X.-F. Zhang, Q. Sun, Y.-C. Wen, W.-M. Liu, S. Eggert, and A.-C. Ji, *Phys. Rev. Lett.* **110**, 090402 (2013).
- [26] C. Guerlin, E. Brion, T. Esslinger, and K. Mølmer, *Phys. Rev. A* **82**, 053832 (2010).
- [27] B. Olmos, R. González-Férez, and I. Lesanovsky, *Phys. Rev. Lett.* **103**, 185302 (2009).
- [28] C. Emary and T. Brandes, *Phys. Rev. E* **67**, 066203 (2003).
- [29] Y. K. Wang and F. T. Hioe, *Phys. Rev. A* **7**, 831 (1973).
- [30] X.-F. Zhang, R. Dillenschneider, Y. Yu, and S. Eggert, *Phys. Rev. B* **84**, 174515 (2011).
- [31] A. W. Sandvik, *Phys. Rev. B* **59**, R14157(R) (1999).
- [32] O. F. Syljuåsen and A. W. Sandvik, *Phys. Rev. E* **66**, 046701 (2002).
- [33] J. K. Freericks and H. Monien, *Phys. Rev. B* **53**, 2691 (1996).
- [34] T. Wang, X.-F. Zhang, C.-F. Hou, S. Eggert, and A. Pelster, *Phys. Rev. B* **98**, 245107 (2018).
- [35] N. D. Mermin and H. Wagner, *Phys. Rev. Lett.* **17**, 1133 (1966).